

A local refinement purely meshless scheme for time fractional nonlinear Schr\"odinger equation in irregular geometry region

Tao Jiang(蒋涛)†, Rong-Rong Jiang(蒋戎戎), Jin-Jing Huang(黄金晶), Jiu Ding(丁玖), and Jin-Lian Ren(任金莲)
Citation: Chin. Phys. B, 2021, 30 (**2**): 020202. DOI: 10.1088/1674-1056/abc0e0
Journal homepage: http://cpb.iphy.ac.cn; http://iopscience.iop.org/cpb

What follows is a list of articles you may be interested in

Compact finite difference schemes for the backward fractional Feynman-Kac equation with fractional substantial derivative

Jiahui Hu(胡嘉卉), Jungang Wang(王俊刚), Yufeng Nie(聂玉峰), Yanwei Luo(罗艳伟)
Chin. Phys. B, 2019, 28 (**10**): 100201. DOI: 10.1088/1674-1056/ab3af3

Heteroclinic cycles in a new class of four-dimensional discontinuous piecewise affine systems

Wenjing Xu(徐文静), Wei Xu(徐伟), Li Cai(蔡力)
Chin. Phys. B, 2018, 27 (**11**): 110201. DOI: 10.1088/1674-1056/27/11/110201

Improved reproducing kernel particle method for piezoelectric materials

Ji-Chao Ma(马吉超), Gao-Feng Wei(魏高峰), Dan-Dan Liu(刘丹丹)
Chin. Phys. B, 2018, 27 (**1**): 010201. DOI: 10.1088/1674-1056/27/1/010201

Topology optimization using the improved element-free Galerkin method for elasticity

Yi Wu(吴意), Yong-Qi Ma(马永其), Wei Feng(冯伟), Yu-Min Cheng(程玉民)
Chin. Phys. B, 2017, 26 (**8**): 080203. DOI: 10.1088/1674-1056/26/8/080203

Finite-difference time-domain modeling of curved material interfaces by using boundary condition equations method

Jia Lu(卢佳), Huaichun Zhou(周怀春)
Chin. Phys. B, 2016, 25 (**9**): 090203. DOI: 10.1088/1674-1056/25/9/090203

A local refinement purely meshless scheme for time fractional nonlinear Schrödinger equation in irregular geometry region*

Tao Jiang(蒋涛)[1,†], Rong-Rong Jiang(蒋戎戎)[1], Jin-Jing Huang(黄金晶)[1], Jiu Ding(丁玖)[2], and Jin-Lian Ren(任金莲)[1]

[1] *School of Mathematical Sciences, Yangzhou University, Yangzhou* 225002, *China*
[2] *Department of Mathematics, University of Southern Mississippi, Hattiesburg, MS* 39406-5045, *USA*

(Received 8 July 2020; revised manuscript received 3 September 2020; accepted manuscript online 14 October 2020)

A local refinement hybrid scheme (LRCSPH-FDM) is proposed to solve the two-dimensional (2D) time fractional nonlinear Schrödinger equation (TF-NLSE) in regularly or irregularly shaped domains, and extends the scheme to predict the quantum mechanical properties governed by the time fractional Gross–Pitaevskii equation (TF-GPE) with the rotating Bose–Einstein condensate. It is the first application of the purely meshless method to the TF-NLSE to the author's knowledge. The proposed LRCSPH-FDM (which is based on a local refinement corrected SPH method combined with FDM) is derived by using the finite difference scheme (FDM) to discretize the Caputo TF term, followed by using a corrected smoothed particle hydrodynamics (CSPH) scheme continuously without using the kernel derivative to approximate the spatial derivatives. Meanwhile, the local refinement technique is adopted to reduce the numerical error. In numerical simulations, the complex irregular geometry is considered to show the flexibility of the purely meshless particle method and its advantages over the grid-based method. The numerical convergence rate and merits of the proposed LRCSPH-FDM are illustrated by solving several 1D/2D (where 1D stands for one-dimensional) analytical TF-NLSEs in a rectangular region (with regular or irregular particle distribution) or in a region with irregular geometry. The proposed method is then used to predict the complex nonlinear dynamic characters of 2D TF-NLSE/TF-GPE in a complex irregular domain, and the results from the posed method are compared with those from the FDM. All the numerical results show that the present method has a good accuracy and flexible application capacity for the TF-NLSE/GPE in regions of a complex shape.

Keywords: Caputo fractional derivative, nonlinear Schrödinger/Gross–Pitaevskii equation, corrected smoothed particle hydrodynamics, irregularly domain

PACS: 02.60.–x, 02.70.–c, 03.65.Ge **DOI:** 10.1088/1674-1056/abc0e0

1. Introduction

In recent years, fractional differential operators have a wide range of applications in engineering and science because they can accurately describe the complex dynamic behaviors in the real world, such as the viscoelasticity procedure, the fluid mechanics, the electrostatics, and other physical events.[1–9] Moreover, the integer nonlinear Schrödinger equation is usually used to describe some physical phenomena in quantum mechanics,[10–16] in which the Gross–Pitaevskii equation (GPE) is one of the most important nonlinear Schrödinger equations. As the fractional calculus receives more and more attention, fractional quantum mechanical phenomena have been discovered in the literature[17,18] and then the fractional nonlinear Schrödinger equation has become an important equation for describing the fractional quantum mechanical character.[5,19–25] Subsequently, some fractional nonlinear Schrödinger equations (FNLSE) have been studied for different mechanical properties.[19] Although the theoretical analysis for fundamental fractional Schrödinger equations is still being carried on, it is very difficult to obtain analytical solutions for most of FNLSEs[5,26–30] Hence, the design of a highly-efficient and accurate numerical method to find approximate solutions for FNLSEs is necessary and important in practice. Presently, many kinds of numerical methods[23–27,31–42] have been proposed for the numerical solutions of time fractional nonlinear Schrödinger equations (TF-NLSEs), such as the finite difference method (FDM), finite element method (FEM) and local discontinuous Galerkin (LDG) method, *etc*. The purpose of this paper is to study the TF-NLSE numerically.

Meshless techniques have gradually attracted researchers' attention and been extensively applied to various PDEs,[43–53] because the meshless method does not need mesh generation or reconstruction required in grid-based methods. There are some common meshless methods,[43–47,51,52] such as the conventional SPH (TSPH),[47] corrected SPH (CSPH),[47–50] EFG,[51,52] MLS,[43] RBFs,[44,46] MLPG,[53] FPM, RKPM,[52] *etc*. Although the above meshless methods have been widely used to simulate various fluid/solid mechanical problems,[47,51,52] the meshless technique is rarely used for the TF-NLE.[46,50,53–55] As a purely meshless particle TSPH or CSPH method without completely depending on grids has been extensively used for many kinds of fluid dynamic fields,[47–50,56–65] it has not yet been applied to TF-

*Project supported by the National Natural Science Foundation of China (Grant Nos. 11501495, 51779215, and 11672259), the Postdoctoral Science Foundation of China (Grant Nos. 2015M581869 and 2015T80589), and the Jiangsu Government Scholarship for Overseas Studies, China (Grant No. JS-2017-227).

†Corresponding author. E-mail: jtrjl_2007@126.com

© 2021 Chinese Physical Society and IOP Publishing Ltd

NLSEs to the best of our knowledge. The CSPH has higher accuracy and better stability than the TSPH, and it is easier to implement in programming than other meshless methods (for example the EFG, MLPG, RBFs, *etc*.).

For the above reason, the main aim of the present paper is to propose a hybrid scheme (named LRCSPH-FDM which is a local refinement corrected SPH method coupled with FDM) for 2D TF-NLSEs in a complex region with irregular geometry by combining the FDM for the Caputo time fractional derivative[66] and the CSPH[50,59] with a new kernel function[63] for spatial derivatives. Meanwhile, the local refinement particle technique is also adopted to reduce the numerical error, and the parallel technique[50,59] is introduced to enhance the computational efficiency. To further demonstrate the capability of the proposed LRCSPH-FDM, the numerical solutions of the challenging time fractional Gross–Pitaevskii equation (TF-GPE) with a potential and a rotation term in an irregularly shaped domain is investigated by the present LRCSPH-FDM. It is worth noting that the main idea of this work has much more progress than that in Ref. [51]. There are three main differences as follows. First, this work focuses on the time fractional nonlinear Schrödinger equation (TF-NLSE) which is different from the time integral nonlinear Schrödinger equation in Ref. [51]. There is a wide range of application in physics, where the TF-NLSE can be used to describe many quantum phenomena[67] but the time integral nonlinear Schrödinger equation cannot. Also, the merits of corrected SPH (which was easily used in irregular complex domains but can be locally refined if need be) are not described well or sufficiently in Ref. [51]. This paper emphasizes the particle characteristics of SPH, so the simulation domain can be locally refined in any areas if need be. Then the SPH scheme can be used in various complex domains (see Fig. 1) which are not simulated in Ref. [51]. Last but not least, the time fractional derivative is much more difficult to obtain than time integral derivative. In $L1-2$ scheme.[66] The results of all former time steps are needed to simulate the current result, but to simulate the integral results only one former time step result is used. So, this method needs to occupy more memory spaces when time increases than that in Ref. [51]. The MPI parallel technique is used in 2D examples to enhance the computation efficiency. In a word, this work simulates the time fractional nonlinear Schrödinger equation in complex domains and the merits of LRCSPH-FDM are demonstrated through the examples.

The rest of this work is organized as follows. The 2D TF-NLSE/GPE with initial/boundary conditions is described in Section 2. The proposed particle scheme for 2D TF-NLSEs based on the local refinement CSPH and FDM is given in Section 3. Section 4 demonstrates the numerical convergence of the proposed method for 2D TF-NLSEs with different cases of the particle distribution in a rectangular or irregularly shaped domain. An extended application of the proposed particle method for 2D TF-NLSE/GPEs in regular/irregular domains is illustrated and discussed in Section 5. Section 6 gives some remarks and conclusions.

2. Time fractional nonlinear Schrödinger equation

We consider the time fractional nonlinear Schrödinger equation (TF-NLSE)[46]

$$\begin{aligned} &\mathrm{i}\frac{\partial^\alpha u(\boldsymbol{x},t)}{\partial t^\alpha}+\beta\Delta u(\boldsymbol{x},t)+V_d(\boldsymbol{x})u(\boldsymbol{x},t)+\lambda|u(\boldsymbol{x},t)|^2u(\boldsymbol{x},t)\\ &=f(\boldsymbol{x},t),\quad \boldsymbol{x}\in\Omega,0\le t\le T \end{aligned} \tag{1}$$

with the initial value condition $u(\boldsymbol{x},0)=w(\boldsymbol{x})$ and the boundary value condition

$$u(\boldsymbol{x},t)=h(\boldsymbol{x},t),\quad \boldsymbol{x}\in\partial\Omega, \tag{2}$$

where $0<\alpha<1$, $u(\boldsymbol{x},t)$ is a complex-valued wave function with the spatial variable $\boldsymbol{x}=(x)$ or $\boldsymbol{x}=(x,y)$, Δ is the d-dimensional Laplace operator (d =1,2), $\mathrm{i}=\sqrt{-1}$ is the imaginary unit, Ω is the simulated domain and $\partial\Omega$ is its boundary, λ is a real constant describing the interaction. The potential term[10,12] $V_d(\boldsymbol{x})$ is a real-valued function that takes the form

$$V_d(\boldsymbol{x},t)=\begin{cases} x^2/2, & d=1,\\ (\gamma_x^2x^2+\gamma_y^2y^2)/2, & d=2. \end{cases} \tag{3}$$

There are several definitions of fractional derivatives, among which the Riemann–Liouville and Caputo fractional derivatives are two of the most used ones in fractional calculus (see Refs. [1,27,46]). In this paper, we use the Caputo fractional derivative.

The Caputo fractional derivative of order α is defined as

$$\begin{aligned} {}_0^cD^\alpha f(x) &= \frac{1}{\Gamma(m-\alpha)}\int_0^x(x-\xi)^{m-\alpha-1}f^{(m)}(\xi)\,\mathrm{d}\xi,\\ &\quad m-1<\alpha<m. \end{aligned} \tag{4}$$

So the Caputo time fractional derivative of order α ($0<\alpha<1$) takes the form

$${}_0^cD_t^\alpha f(t)=\frac{1}{\Gamma(1-\alpha)}\int_0^t\frac{f'(\xi)}{(t-\xi)^\alpha}\,\mathrm{d}\xi=\frac{\partial^\alpha f(t)}{\partial t^\alpha}. \tag{5}$$

Also, the Caputo fractional derivative satisfies

$${}_0^cD^\alpha x^p=\frac{\Gamma(p+1)}{\Gamma(p+1-\alpha)}x^{p-\alpha}. \tag{6}$$

The Gamma function $\Gamma(z)$ is

$$\Gamma(z)=\int_0^\infty x^{z-1}\,\mathrm{e}^{-x}\,\mathrm{d}x, \tag{7}$$

where z is in the complex domain, and has the following properties:

(i) $\Gamma(z+1)=z\Gamma(z)$,

(ii) for any $n\in N$, the set of positive integers, $\Gamma(n)=(n-1)!$,

(iii) $\Gamma(0)=1$, $\Gamma(1/2)=\sqrt{\pi}$.

3. Local refinement approximate scheme (LRCSPH-FDM)

3.1. Scheme for time fractional derivative

At present, two approximation schemes for the Caputo time fractional derivative have been proposed and used widely to solve time factional differential equations, which are called the $L1$ method with $o(\tau^{2-\alpha})$-order[4–9] and $L1-2$ method with $o(\tau^{3-\alpha})$-order,[66] respectively. Here, the $L1-2$ scheme is adopted.

Taking the 1D case, let the positive integers M and Nbe given, set the time step $\tau = T/M$ and the space step $h' = L/N$, and define the space nodes $x_i = ih'$ with $0 \le i \le N$ and the time nodes $t_n = n\tau$ with $0 \le n \le M$. Then the $L1-2$ formula for the Caputo fractional derivative (5)[1] can be obtained as follows:

$$
\begin{aligned}
&{}_0^cD_t^\alpha u^k \\
&= \frac{\tau^{-\alpha}}{\Gamma(2-\alpha)}\left[c_0^\alpha u^k - \sum_{j=1}^{k-1}(c_{k-j-1}^\alpha - c_{k-j}^\alpha)u^j - c_{k-1}^\alpha u^0\right], \quad (8)
\end{aligned}
$$

where $0 \le j \le k-1$, and for $k \ge 2$

$$
c_j^\alpha = \begin{cases} a_0^\alpha + b_0^\alpha, & j = 0, \\ a_j^\alpha + b_j^\alpha - b_{j-1}^\alpha, & 1 \le j \le k-2, \\ a_j^\alpha - b_{j-1}^\alpha, & j = k-1, \end{cases} \quad (9)
$$

where $a_j^\alpha = (j+1)^{1-\alpha} - j^{1-\alpha}$, $b_j^\alpha = [1/(2-\alpha)]((j+1)^{2-\alpha} - j^{2-\alpha}) - (1/2)((j+1)^{1-\alpha} + j^{1-\alpha})$, $c_0^\alpha = a_0^\alpha = 1$ $(k=1)$. The properties of the coefficientsa_j^α, b_j^α, c_j^α that need satisfied are available from Ref. [66].

3.2. CSPH scheme for space derivatives

3.3. Conventional SPH scheme

In the conventional SPH simulation, the kernel function[47–50] is first used for integral interpolates. Secondly, the simulated domain Ω is discretized into a finite number of particles by the SPH method,[47] where each particle has its own physical quantities such as the density, mass and the temperature, which depend on the problem solved. Finally, the integral form of the kernel function is approximately obtained by the particle discretization.

The integral representation of the function $u(\boldsymbol{x})$ and the derivative of the function $\nabla u(x)$ at the point $\boldsymbol{x} = (x, y)$ can be obtained by the kernel function W and the kernel function derivative ∇W as follows:[47,50]

$$
\langle u(\boldsymbol{x})\rangle = \int_\Omega u(\mathbf{x}')W(\boldsymbol{x}-\boldsymbol{x}', h)\,\mathrm{d}\boldsymbol{x}', \quad (10)
$$

$$
\begin{aligned}
\langle \nabla\cdot u(\boldsymbol{x})\rangle &= \int_\Omega \nabla\cdot\left[u(\boldsymbol{x}')W(\mathrm{x}-\boldsymbol{x}', h)\right]\mathrm{d}\boldsymbol{x}' \\
&\quad - \int_\Omega u(\boldsymbol{x}')\cdot\nabla W(\boldsymbol{x}-\boldsymbol{x}', h)\,\mathrm{d}\boldsymbol{x}'. \quad (11)
\end{aligned}
$$

In this paper, the double cosine smoothing function[63] is considered as

$$
\begin{aligned}
&W(R,h) \\
&= \alpha_d \times \begin{cases} 4\cos\left(\dfrac{\pi}{\kappa}R\right) + \cos\left(\dfrac{2\pi}{\kappa}R\right) + 3, & 0 \le R \le \kappa, \\ 0, & \kappa < R, \end{cases} \quad (12)
\end{aligned}
$$

where h is the smoothing length in the kernel function W, $R = x_{ij}/h$, $x_{ij} = |\boldsymbol{x}_i - \boldsymbol{x}_j|$, and the coefficient $\alpha_d = 1/(6\kappa h)$, $\pi/((3\pi^2-16)\kappa^2h^2)$, and $\pi/((4\pi^2-30)\kappa^3h^3)$ in 1D/2D/3D, respectively. The parameter κ is chosen as $2 \le \kappa \le 3$, the support domain size is κh, and h is chosen from $0.9d_0$ to $1.3d_0$ in the following simulation. The advantage of this kernel function can be found in Ref. [63]. Moreover, the kernel function W often satisfies the following conditions:[47,50] (i) the normalization property $\int_\Omega W(\boldsymbol{x}-\boldsymbol{x}', h)\,\mathrm{d}\boldsymbol{x}' = 1$; (ii) the Dirac function property $\lim_{h\to 0} W(|\boldsymbol{x}-\boldsymbol{x}'|, h) = \delta(|\boldsymbol{x}-\boldsymbol{x}'|)$; (iii) the compactness property $W(|\boldsymbol{x}-\boldsymbol{x}'|, h) = 0$ when $|\boldsymbol{x}-\boldsymbol{x}'| > \kappa h$; (iv) the symmetry property $\int_\Omega (\boldsymbol{x}'-\boldsymbol{x})W(\boldsymbol{x}-\boldsymbol{x}', h)\,\mathrm{d}\boldsymbol{x}' = 0$, which means that W is an even function.

In the simulation, for the particle j within the support domain of particle i, its volume is $v_j = m_j/\rho_j$ (the real-valued constants m_j and ρ_j are the mass and density of the particle j respectively), and then the particle approximate formulas for any particle i at the point $\boldsymbol{x}$ are[50]

$$
u_i = \sum_j^{N_i} u_j W_{ij} v_j, \quad (13)
$$

$$
\left(\frac{\partial u}{\partial \boldsymbol{x}_i}\right) = \sum_j^{N_i}(u_j - u_i)\nabla_i W_{ij} v_j, \quad (14)
$$

where $W_{ij} = W(|\boldsymbol{x}_i - \boldsymbol{x}_j|, h)$, $\nabla_i W_{ij} = \partial W(|\boldsymbol{x}_i - \boldsymbol{x}_j|, h)/\partial \boldsymbol{x}_i$, and $\nabla_i W_{ij}$ satisfies $\nabla_i W_{ij} = -\nabla_j W_{ij}$. The positive integer N_i represents the neighbor particle number within the support domain of particle i.

3.4. Corrected SPH scheme

There have arisen the problems with low accuracy and instability[47,49,56] as the conventional SPH method is used near the boundary of the domain, or in the case of irregular particle distributions. Some improved SPH methods have been proposed to enhance the numerical accuracy and stability by using the Taylor expansion.[47–50,56] A corrected SPH (CSPH) scheme for the first-order derivative with two-order accuracy without kernel derivatives has been proposed in Refs. [59,62], which can perform well even in the region of non-uniform particle distributions.[50] So far, the above CSPH has not been used to solve the fractional differential problem to the best of our knowledge. In this work, the CSPH scheme combining the FDM scheme (8) is used to approximate the TF-NLSE (1), in which the space derivative of Eq. (1) is discretized by the CSPH. Then, the conventional SPH scheme (14) for the first-order derivative can be corrected as

$$
\left(\frac{\partial u}{\partial \boldsymbol{x}_i}\right) = \sum_j^{N_i}(u_j - u_i)\nabla_i^c \hat{W}_{ij} v_j, \quad (15)
$$

and $\nabla_i^c \hat{W}_{ij} v_j$ is obtained by solving the following system of equation:

$$A^s \begin{pmatrix} \partial \hat{W}_{ij}^c / \partial x_i \\ \partial \hat{W}_{ij}^c / \partial y_i \end{pmatrix} = \begin{pmatrix} x_{ji} W_{ij} \\ y_{ji} W_{ij} \end{pmatrix}, \tag{16}$$

where $A^s = \sum_j^{N_i} \left(W_{ij} \begin{pmatrix} x_{ji}x_{ji} & y_{ji}x_{ji} \\ x_{ji}y_{ji} & y_{ji}y_{ji} \end{pmatrix} v_j \right)$, $x_{ji} = x_j - x_i$, $y_{ji} = y_j - y_i$.

For the second-order derivative $\partial^2 u / \partial \boldsymbol{x}_i^2$, it is firstly discomposed into two first-order derivatives. Secondly, the above corrected scheme (15) for the first-order derivative is adopted continuously to approximate the above second-order derivative. That is,

$$\left(\frac{\partial^2 u}{\partial \boldsymbol{x}_i^2} \right) = \sum_j \left(\left(\frac{\partial u}{\partial \boldsymbol{x}} \right)_j - \left(\frac{\partial u}{\partial \boldsymbol{x}} \right)_i \right) \nabla_i^c \hat{W}_{ij} v_j. \tag{17}$$

From the above procedures, it can be seen that neither the CSPH scheme (15) nor the CSPH scheme (17) involves kernel function derivative, which offers some advantages over other improved SPH methods.[59,62] Also, the CSPH method has a better flexibility than a class of grid-based methods (*e.g.*, FDM) due to its own special advantages, for example, an easy implementation of simulations in the case of non-uniform particle distributions or irregular computing domains. In other words, the local refinement approach is suitably and easily implemented for reducing the numerical error in the present particle method, but it is complicated in the grid-based methods. And then the local refinement particle distribution technique is applied to the boundary and specified parts of the computing region when the CSPH scheme (15) combined with the FDM scheme (8) is proposed for the TF-NLSE, named the "LRCSPH-FDM" scheme. The above viewpoints will be demonstrated in the following (Section 4) by the numerical simulation for several examples, involving the numerical convergence rate and the flexibility of the proposed method. It is regrettable that a strictly unified theory of the particle method has not been developed well[47,52,56] due to the influence of some empirical theory parameters.

To show the calculation process of the LRCSPH-FDM scheme directly, the flowchart is as follows.

Input: The simulation domain Ω (the locally refined domain and the irregular particle distributions areas); the discrete particle numbers N; computation time T; the space step h'; the time step τ; the simulation function u; the kernel function W and its smoothing length h; some physical quantities for particles; the coefficient a, b, c of $L1-2$ scheme.

Output: The approximated solution $u(\boldsymbol{x}_j, T)$.

The detailed algorithm flow:

Step 1 The simulated domain Ω is discretized into N particles and for each particle $\boldsymbol{x}_j$ $(j = 0, 1, \ldots, N-1)$, its neighbor particles are marked. It is noted that Ω has various particle distributions (see Fig. 1) and some of them are difficult to simulate by the grid-based method. Meanwhile, to enhance the computation accuracy, the local refinement scheme is used.

Step 2 Assign the physical quantities for each particle x_j. The initial data are assigned to $u(x_j, t = 0)$.

Step 3 The first-order derivative $\partial u / \partial \boldsymbol{x}_j$ is approximated by formula (15) (combined with formula (16)), noting that the boundary conditions are not considered here.

Step 4 Use the result in Step 3 as the initial value, then the second-order derivative

$$\frac{\partial^2 u}{\partial \boldsymbol{x}_j^2} = \frac{\partial}{\partial \boldsymbol{x}_j} \left(\frac{\partial u}{\partial \boldsymbol{x}_j} \right)$$

is obtained by using formula (15) repeatedly.

Step 5 The first and second-order derivative on the right-hand side are achieved by Steps 2–4 (corrected SPH) and the $L1-2$ scheme (FDM) is used to approximate the time derivative on the left-hand side, the next time step result is obtained to be $u(\boldsymbol{x}_j, t_1)$. Update the results on the boundaries with the boundary conditions.

Step 6 The temporal loop (from Step 3 to Step 5) is continuously implemented until the required computation time is achieved and then the result $u(\boldsymbol{x}_j, T)$ is output.

Moreover, the parallel technique based on the MPI communication is adopted to enhance the computational efficiency in the programming with C++, which is detailed in our pervious researches.[50,59]

4. Numerical accuracy and convergence of LRCSPH-FDM

In this section, the convergence rate and the flexibility of the proposed LRCSPH-FDM for the TF-NLSE are shown by the numerical demonstration. Three 1D/2D examples[31,36,46] with Dirichlet or periodic boundary conditions are considered in a regular or irregular particle distributed region (see Fig. 1). The $L2$-norm error and convergence rate are defined as

$$e_2 = \frac{\sqrt{\sum_{j=0}^{N} (|u_j| - |U_j|)^2}}{\sqrt{\sum_{j=0}^{N} |U_j|^2}}, \tag{18}$$

$$Cr \approx \frac{\log(e_2(d_{02})/e_2(d_{01}))}{\log(d_{02}/d_{01})}, \tag{19}$$

where u_j represents the numerical solution, U_j is the exact solution, and d_{01} and d_{02} are two different initial particle distances.

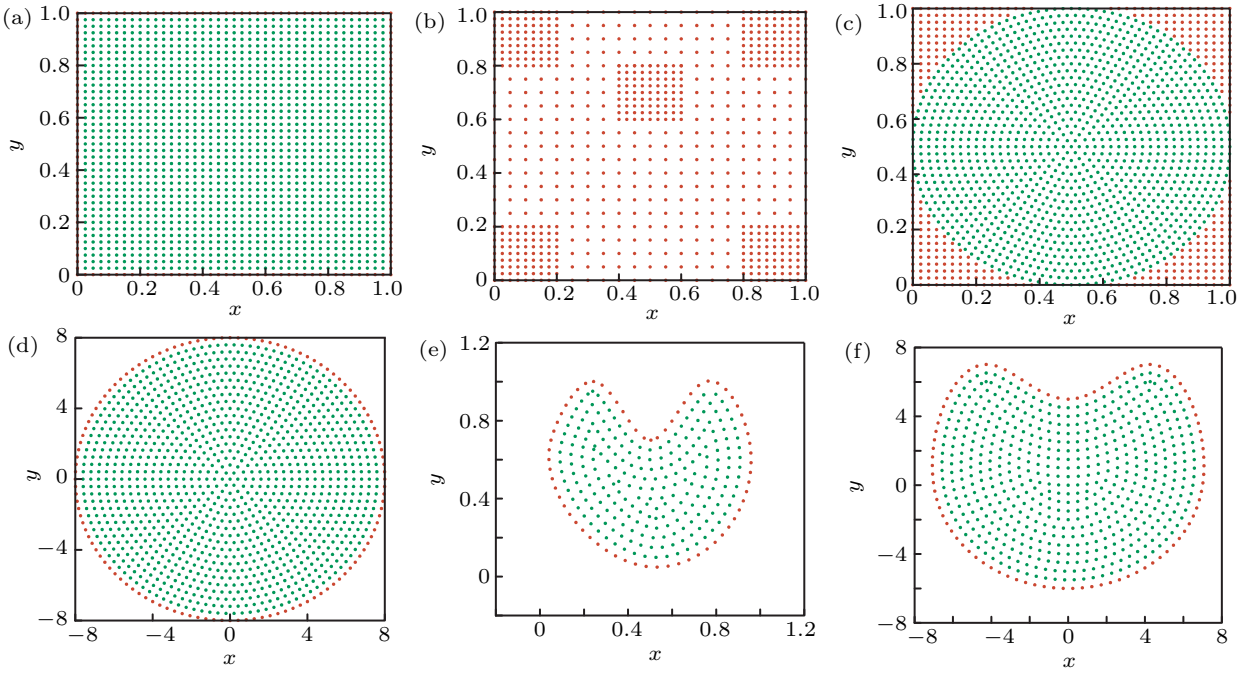


Fig. 1. Sketches of all computational regions with different particle distributions in the whole numerical solvers.

It is worth noting that figure 1 shows the sketches of all particle distributed cases in regular or irregular computing domains in the whole numerical solvers of Sections 4 and 5. Panel 1(a) shows the case of uniform particle distribution in a rectangular domain. Panels 1(b) and 1(c) display two cases of non-uniform particle distributions in rectangular domains, involving the local refinement case of panels (b). Panels (d)–(f) are for the cases of non-uniform particle distributions in irregular computing regions, which are obtained by the Abaqus software.

Example 1 (1D TF-NLSE) We consider the 1D TF-NLSE

$$\mathrm{i}\frac{\partial^\alpha u(x,t)}{\partial t^\alpha}+\frac{\partial^2 u(x,t)}{\partial x^2}+|u(x,t)|^2u(x,t)=f(x,t),\quad x\in[0,1]$$

with the periodic boundary value condition $u(0,t)=u(1,t)=\mathrm{i}t^2$, $t\in[0,1]$ and the initial value condition $u(x,0)=0$. The source term $f(x,t)$ is

$$\begin{aligned}f(x,t) &= -\frac{2t^{2-\alpha}}{\Gamma(3-\alpha)}\cos(2\pi x)+(t^6-4\pi^2t^2)\sin(2\pi x)\\ &\quad+\mathrm{i}\left(\frac{2t^{2-\alpha}}{\Gamma(3-\alpha)}\sin(2\pi x)+(t^6-4\pi^2t^2)\cos(2\pi x)\right)\end{aligned}$$

and the exact solution is $u(x,t)=t^2(\sin(2\pi x)+\mathrm{i}\cos(2\pi x))$.

Example 2 (1D coupled TF-NLSE) Consider the following 1D non-homogeneous coupled time fractional nonlinear Schrödinger equation:

$$\begin{aligned}&\mathrm{i}\frac{\partial^\alpha u}{\partial t^\alpha}+\mathrm{i}u_x+u_{xx}+u+v+2(|u|^2+|v|^2)u=f_1(x,t),\\ &\mathrm{i}\frac{\partial^\alpha v}{\partial t^\alpha}-\mathrm{i}v_x+v_{xx}+u-v+4(|u|^2+|v|^2)v=f_2(x,t),\end{aligned}$$

where functions $f_1(x,t)$, $f_2(x,t)$ are

$$\begin{aligned}f_1(x,t) &= -\frac{2t^{2-\alpha}}{\Gamma(3-\alpha)}\sin x+4t^6\cos x\\ &\quad+\mathrm{i}\left(\frac{2t^{2-\alpha}}{\Gamma(3-\alpha)}\cos x+4t^6\sin x\right),\\ f_2(x,t) &= -\frac{2t^{2-\alpha}}{\Gamma(3-\alpha)}\sin x+8t^6\cos x\\ &\quad+\mathrm{i}\left(\frac{2t^{2-\alpha}}{\Gamma(3-\alpha)}\cos x+8t^6\sin x\right).\end{aligned}$$

The above equations have the computing domain $[0,2\pi]$ and the analytical solution is $u(x,t)=t^2(\cos x+\mathrm{i}\sin x)$, and $v(x,t)=t^2(\cos x+\mathrm{i}\sin x)$. The initial data and the boundary condition can be obtained by the above theoretical solution.

Through the simulations of Examples 1 and 2, the numerical convergence rate and the flexibility of the proposed method for the 1D TF-NLSE are shown in Figs. 2 and 3 and Tables 1 and 2. Figure 2 shows the changes of curves $\mathrm{Re}(u)$ and $\mathrm{Im}(u)$ obtained by the present method for Example 1 with $\alpha=0.7$ at different times. The particle number $N=41$ and time step $\mathrm{d}t=1.0\times10^{-4}$. The present numerical results including the real and imaginary part of u accord well with the analytical solutions. As the time increases, the real part expands in the sinusoidal form and the imaginary part expands in the cosine form. The error (e_2) and convergence rate (C_r) of the modulus, real and imaginary part of u obtained by using the proposed method for Example 1 ($\alpha=0.7$ at $t=1$) are demonstrated in Table 1, and the advantage of local refinement particle distributions is illustrated in Table 2. It can be seen that the proposed method has almost second-order numerical accuracy for solving the 1D TF-NLSE (see Table 1).

In Table 2, the local refinement regions $[0,0.1]$ and $[0.9,1]$ are set to be the initial particle distance $d_0 = 1/80$, and the other region is set to be $d_0 = 1/40$. The error of the local refinement case is obviously smaller than that of the coarse case at different times. For the proposed purely meshless particle method, the local refinement technique can be easily implemented in simulation and it can enhance the numerical accuracy without adding more calculations. To further investigate the accuracy and ability of the proposed method for the 1D TF-NLSE, the 1D coupled TF-NLSE of Example 2 with two interacting nonlinear packets is simulated as indicated in Fig. 3. It is accurate to capture the interaction between two nonlinear waves by the proposed method, and the evolution of the wave function versus time is also accurately simulated.

In a word, the proposed purely meshless method is accurate and flexible for solving the 1D TF-NLSE.

Next, the numerical convergence rate and flexibility of the present method for the 2D TF-NSLE problem are demonstrated by the following simulation of Example 3 in rectangular or irregular computing domains.

Table 1. Values of error (e_2) and convergence rate (C_r) of the modulus, real and imaginary parts of u obtained by the proposed method for Example 1 with $\alpha = 0.7$ at $t = 1$.

$\alpha = 0.7$	$N = 41$	$N = 61$	$N = 81$
Im(u)	0.0230	0.011	0.0064
C_r		1.82	1.88
Re(u)	0.038	0.0174	0.0099
C_r		1.93	1.96
$\|u\|$	0.0309	0.0144	0.00821
C_r		1.88	1.95

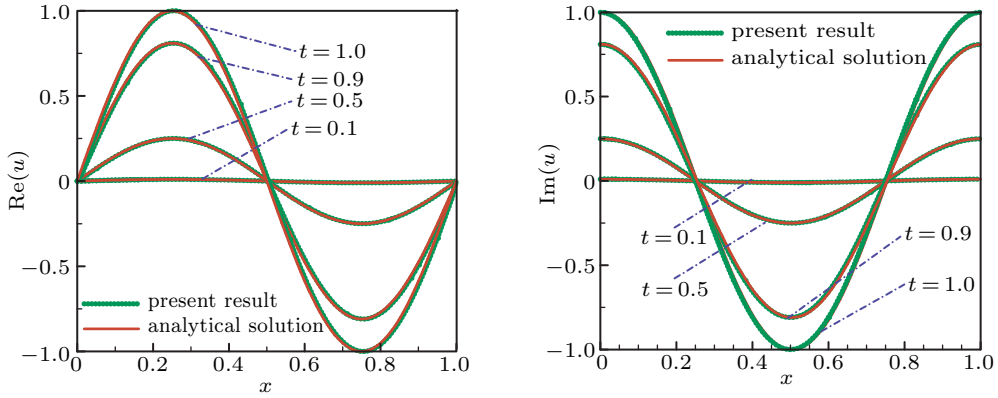


Fig. 2. Changes of curves of Re(u) and Im(u) obtained by the present method for Example 1 with $\alpha = 0.7$ at different times.

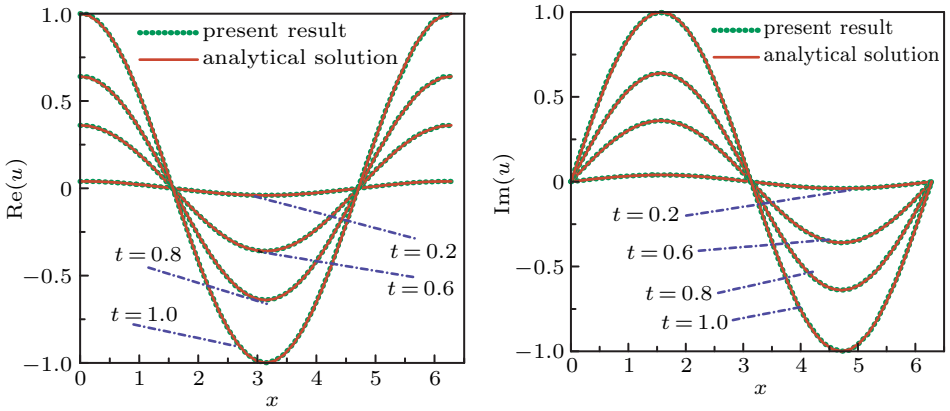


Fig. 3. Changes of curves of Re(u) and Im(u) obtained by the present method for Example 2 with $\alpha = 0.7$ at different times.

Table 2. Comparison of errors (e_2) of $|u|$ obtained by the proposed method between two particles' distributions of coarse case and local refinement case for Example 1 with $\alpha = 0.7$ at different times.

Time	0.1	0.3	0.5	0.7	1.0
Coarse case	0.009587	0.011544	0.0173111	0.0226251	0.0309301
Local refinement case	0.003181	0.005945	0.0093217	0.0135954	0.0178245

Example 3 (2D TF-NLSE) Consider the 2D time-fractional nonlinear Schrödinger equation

$$\mathrm{i}\frac{\partial^\alpha u}{\partial t^\alpha} + \frac{1}{2}\frac{\partial^2 u}{\partial x^2} + \frac{1}{2}\frac{\partial^2 u}{\partial y^2} - |u|^2 u = f(x,y,t)$$

with the nonlinear term

$$f(x,y,t) = \left[\frac{6\mathrm{i}t^{3-\alpha}}{\Gamma(4-\alpha)} - t^3 - t^9\right](\cos(x+y) + \mathrm{i}\sin(x+y)).$$

The analytical solution $u(x,y,t) = t^3(\cos(x+y) + \mathrm{i}\sin(x+y))$

in the rectangular region $(x,y) \in [0,1] \times [0,1]$ or in the irregular region (panels (e)) in Fig. 1 is considered in this subsection. The initial data and boundary condition can be achieved by the above exact solution.

In the simulation of Example 3 with $\alpha = 0.7$, the particle distributions of panels (a), (b), and (c) in Fig. 1 in the rectangular region and the particle distribution panel (e) of Fig. 1 in the irregular one (which is obtained by the Abaqus software) are all used to show the accuracy and the extended flexibility of the proposed method for the 2D TF-NLSE (see Figs. 4–6 and Tables 3 and 4). Meanwhile, the advantage of the purely meshless particle method over the gird-based method (*e.g.*, FDM) is also obviously demonstrated. The curves of the real and imaginary part of $u(0.3,y)$ obtained by the proposed method for Example 3 with $\alpha = 0.7$ at $t = 0.2$ are shown in Fig. 4. The present numerical results accord well with the exact solution. The numerical convergence rate and computing errors of the proposed method for the 2D TF-NLSE with particle distributions [panels (a) and (b) in Fig. 1] are illustrated in Tables 3 and 4, respectively. From Figs. 4–6 and Tables 3 and 4, we can obtain that (i) the proposed method has a numerical accuracy of about 1.8 for the 2D TF-NLSE; (ii) the present method is accurate and can be flexibly used to simulate the 2D TF-NLSE with non-uniform particle distributions (panels (b) and (c) in Fig. 1) in rectangular regions or an irregular domain (panel (e) in Fig. 1); (iii) the local refinement technique in the proposed method is feasible and efficient ($[0,0.2] \times [0,0.2]$, $[0.8,1.0] \times [0,0.2]$, $[0,0.2] \times [0.8,1]$, $[0.8,1] \times [0.8,1]$, $[0.4,0.6] \times [0.6,0.8]$ are the local refinement regions); (iv) the contour of the wave in the 2D TF-NLSE with non-uniform particle distributions can be exactly obtained by the proposed purely meshless method.

Table 3. Values of error (e_2) and convergence rate (C_r) of modulus, real and imaginary parts of u obtained by the proposed method for Example 3 with $\alpha = 0.7$ at $t = 0.2$.

$\alpha = 0.7$	$N = 41^2$	$N = 61^2$	$N = 81^2$
Im(u)	0.000558	0.000277	0.000165
C_r		1.73	1.80
Re(u)	0.001970	0.000985	0.000583
C_r		1.71	1.82
$\lvert u\rvert$	0.001260	0.000628	0.000372
C_r		1.72	1.82

Table 4. Comparison of error (e_2) of $|u|$ obtained by using the proposed method between two particle distribution cases of panels (a) and (b) in Fig. 1 for Example 3 with $\alpha = 0.7$ at different times.

Time	0.05	0.1	0.15	0.2
Coarse case panels (a) of Fig. 1	0.0010925	0.00126013	0.00143292	0.0053836
Local refinement case panels (b) of Fig. 1	0.0007278	0.00079098	0.0008346	0.0039295

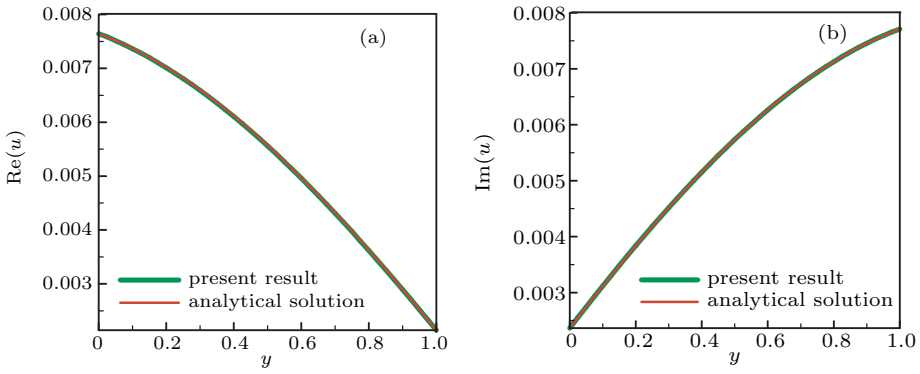


Fig. 4. Curves of (a) real and (b) imaginary parts of $u(0.3,y)$ for Example 3 with $\alpha = 0.7$ at $t = 0.2$.

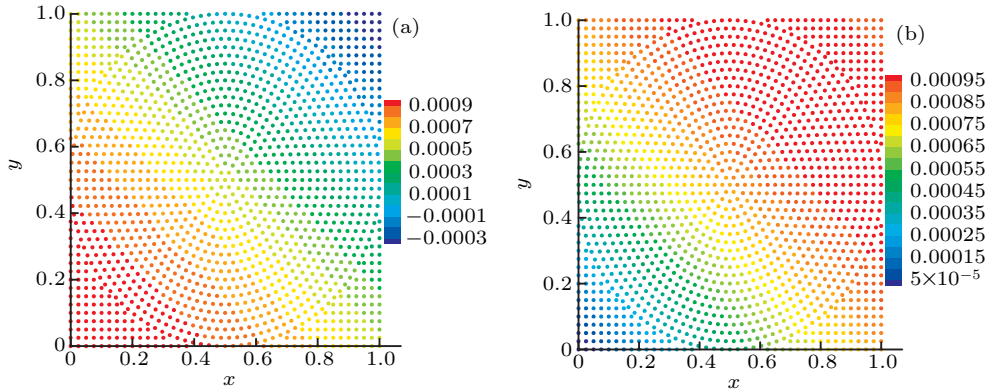


Fig. 5. Contours of non-uniform particle distribution panel (c) of Fig. 1 obtained by using the proposed method for Example 3 with $\alpha = 0.7$ at $t = 0.1$: (a) Re(u) and (b) Im(u).

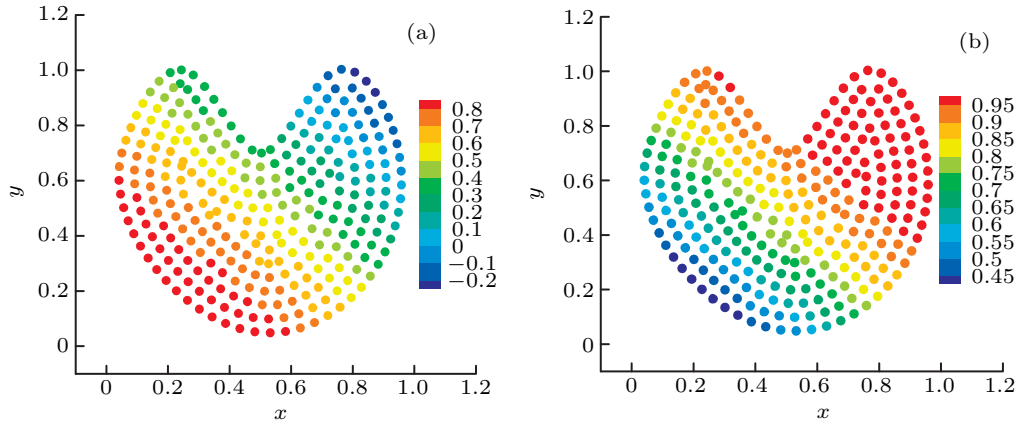


Fig. 6. The contours of the particle distribution panel (e) of Fig. 1 obtained by using the present method for Example 3 on an irregular region with $\alpha = 0.7$ at $t = 1$: (a) Re(u) and (b) Im(u).

To sum up, the proposed particle method has a better numerical accuracy for the 2D TF-NLSE with non-uniform particle distributions panels (b) and (c) in Fig. 3, and a stronger flexibility in extended applications than the FDM for the 2D TF-NLSE in complex domains with an irregular geometry.

5. Numerical investigation for 1D/2D TF-NLSE

In order to further demonstrate the ability and flexibly extended application of the proposed purely meshless method for the TF-NLSE, three classical 1D/2D examples without theoretical solutions are considered and investigated by the present method, and compared with the FDM results.

Example 4 (1D TF-NLSE) Consider the 1D time fractional nonlinear Schrödinger equation

$$\mathrm{i}\frac{\partial^{\alpha} u}{\partial t^{\alpha}} = -u_{xx} + V(x)u + f(|u|^2)u, \quad x \in [-20, 20]$$

with the initial value condition $u(x,0) = u_0(x)$ and the boundary value condition $u(x,t) \to 0$ $(|x| \to \infty)$. The external potential function $V(x) = 0$, the nonlinear term $f(|u|^2)u = 2|u|^2 u + |u|^4 u$ includes general nonlinear effects on u, and the initial data $u_0(x) = \mathrm{e}^{-3(x-2)^2} + \mathrm{e}^{-3(x+2)^2}$.

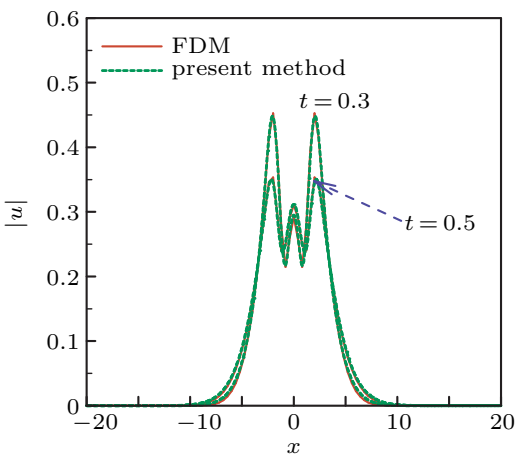


Fig. 7. Comparison between curves of $|u|$ *versus* x, obtained by different methods for Example 4 with $\alpha = 0.7$ at two different times.

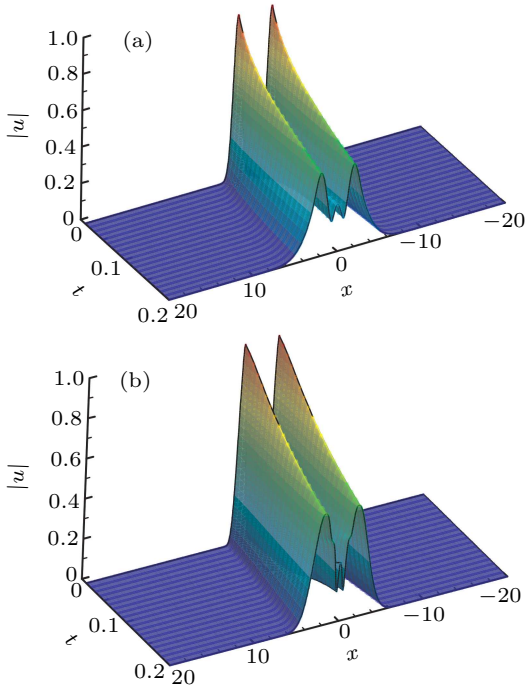


Fig. 8. Evolution of wave $|u|$ with time, obtained by the present method for Example 4 with (a) $\alpha = 0.7$ and (b) $\alpha = 0.95$.

To verify the reliability of the present method for Example 4, figure 7 illustrates the comparisons between $|u|$ values obtained using different methods for Example 4 with $\alpha = 0.7$ at two different times. The present numerical results are closer to the FDM results, which indicates that the proposed method is credible for predicting the wave change versus time in the 1D TF-NLSE. The evolution of wave $|u|$ versus time, obtained by the present method for Example 4 with two different α values, is shown in Fig. 8. Figure 9 shows the curve of wave $|u|$ at t =0.2 with $\alpha = 0.7$ and $\alpha = 0.95$ for showing the difference in nonlinear wave between two different fractional parameters. From Figs. 8 and 9, we can find that i) the crest of the wave decreases as time goes on; ii) it is reliable to predict the evolution of nonlinear waves in the 1D TF-NLSE by the proposed method; iii) the fractional parameter has an important influence on the wave movement; iv) a larger peak value of wave

$|u|$ is achieved when the parameter α increases.

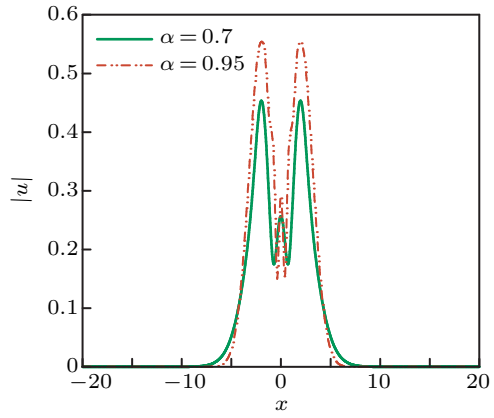


Fig. 9. Waves $|u|$ obtained by the present method for Example 4 at $t = 0.2$ with two different α values.

Example 5 (2D TF-NLSE) Consider the 2D time-fractional nonlinear Schrödinger equation with a periodic condition, which is

$$\mathrm{i}\frac{\partial^\alpha u}{\partial t^\alpha} + \Delta u + \beta |u|^2 = 0, \quad (x,y) \in (0,2\pi) \times (0,2\pi)$$

and the initial data $u(x,y,0) = (1+\sin x)(2+\sin y)$. The periodic size along the x direction and along the y direction are both 2π.

The case of Example 5 with $\alpha = 1$(time integral order) is usually considered to illustrate the extended application and the robustness of a numerical method for the NLSE, which can be seen in Ref. [68]. Figure 10 shows the wave $|u|$ obtained by two different methods for Example 5 at $t = 0.108$ with $\alpha = 1$ (time integral order) and $\alpha = 0.7$ (time fractional order). The initial particle distance $d_0 = 1/60$, time step $\mathrm{d}t = 2.0 \times 10^{-5}$ and $\beta = 1$. To illustrate the difference in result between integral time derivative and fractional time derivative, figure 10 displays the results for time derivative changing with time. The result at $t = 0$ is the initial result, while figure 10(a) shows the result with time integral order ($\alpha = 1$) and figure 10(b) displays the result with time fractional order ($\alpha = 0.7$) when $t = 0.108$. From the results, it can be seen that there is a sharp wave with high value when $\alpha = 1$ and when the time derivative changes to $\alpha = 0.7$ (time fractional derivative), the evolution is quite different. In Fig. 10(b), it turns out to be two small waves. To demonstrate these results, in this work the results from the FDM are compared with those from the LRCSPH-FDM. It is clear that the present numerical results are in agreement with the FDM results, which indicates that a) it is reliable to predict the wave propagation with a periodic boundary condition by the present method; b) the fractional parameter has a significant influence on the wave change in the 2D TF-NLSE; c) the singularity can be obviously observed when$\alpha = 1$, and it is weakened when $\alpha = 0.7$ (see Fig. 10(b)).

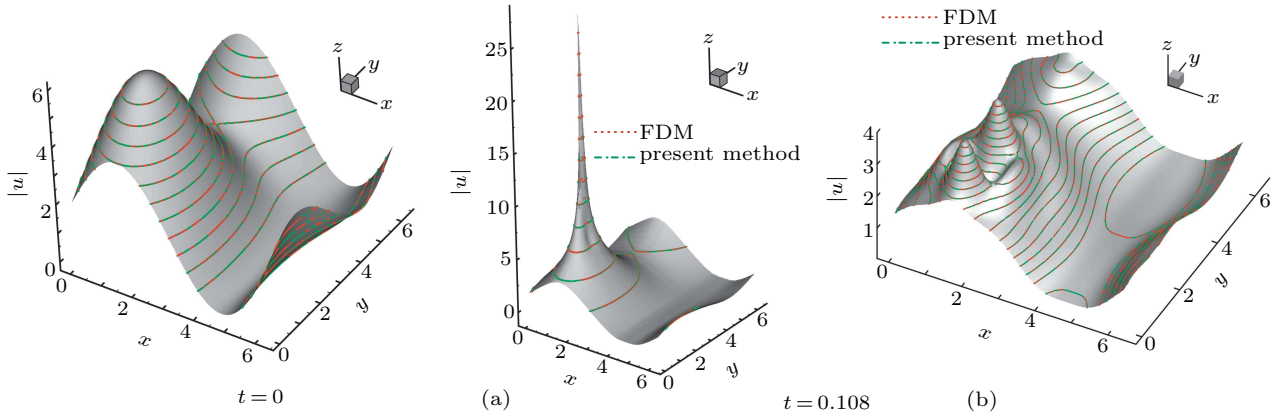


Fig. 10. Waves $|u|$ obtained by using different methods for Example 5 at $t = 0.108$ with (a) $\alpha = 1$ (time integral order); (b) $\alpha = 0.7$ (time fractional order).

Example 6 (2D TF-GPE) Consider the 2D time fractional Gross–Pitaevskii equation with a rotating term

$$\mathrm{i}\frac{\partial^\alpha u}{\partial t^\alpha} = -\frac{1}{2}\nabla^2 u + V_2(\boldsymbol{x})u + \beta_2 |u|^2 u - \mathrm{i}L_z(y\partial x - x\partial y)u,$$

with the initial data

$$u(x,y,0) = \frac{(\gamma_x\gamma_y)^{1/4}}{\sqrt{\pi}} \exp(-(\gamma_x x^2 + \gamma_y y^2)/2.0)$$

and boundary condition $\lim_{|x|\to\infty} u(x,y,t) = 0$. The potential term

$$V(\boldsymbol{x},t) = \frac{(\gamma_x^2 x^2 + \gamma_y^2 y^2)}{2},$$

and the other parameters $\gamma_x = \gamma_y = 1.0$, $L_z = 0.7$, and $\beta_2 = 1.0$.

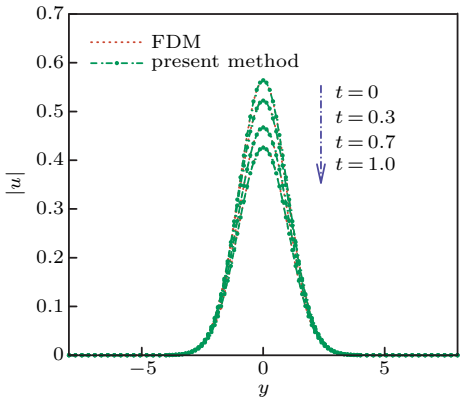


Fig. 11. Comparison of waves $|u(0,y)|$ obtained by different methods for Example 6 with $\alpha = 0.7$.

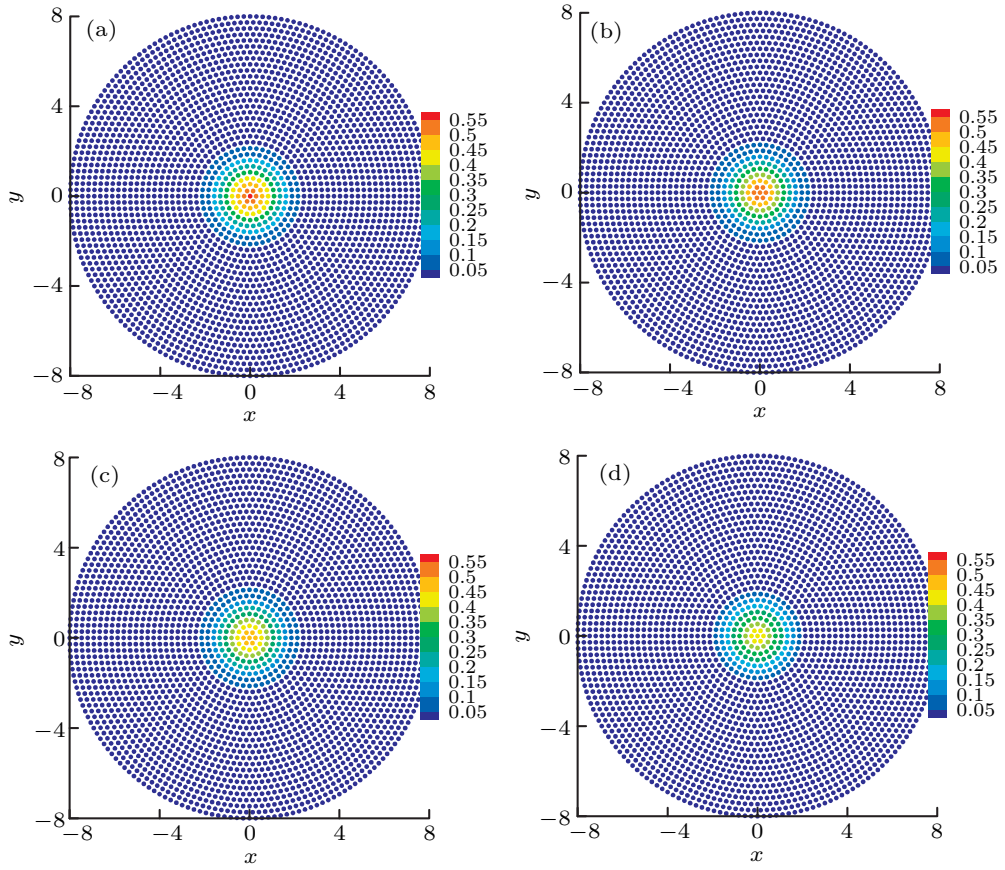


Fig. 12. Contours of wave $|u|$ obtained by the present method for Example 6 for particle distribution panels (d) of Fig. 1 with $\alpha = 0.7$ at different times: (a) $t = 0$, (b) $t = 0.3$, (c) $t = 0.6$, and (d) $t = 1$.

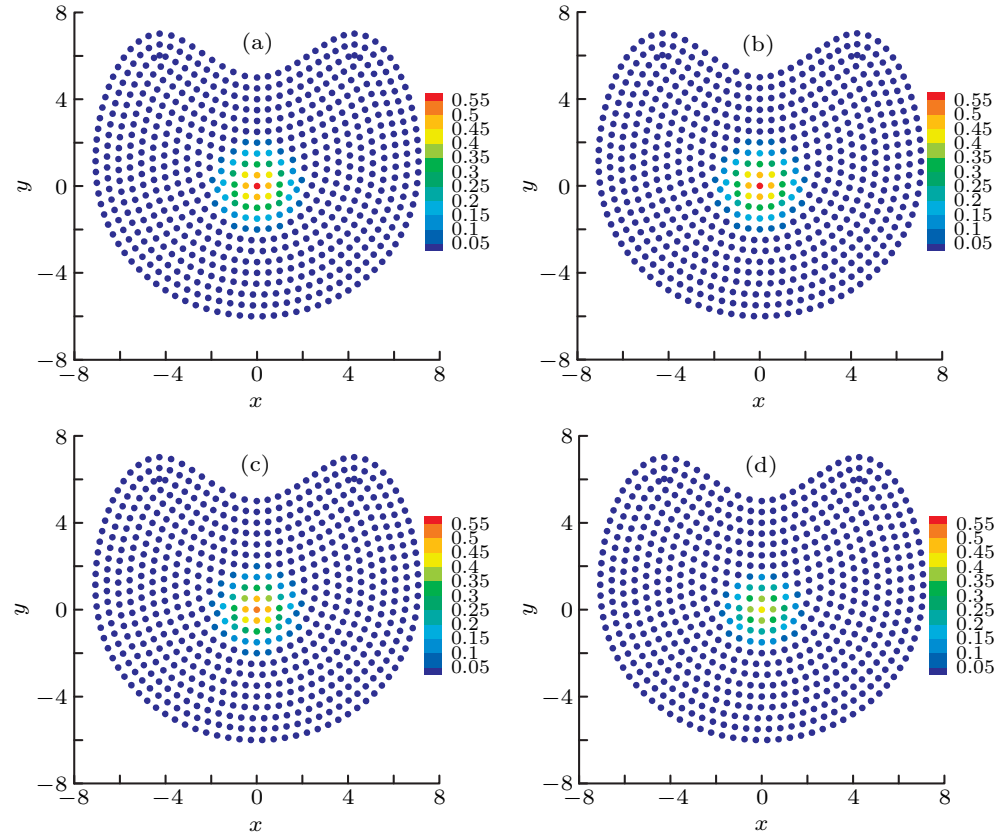


Fig. 13. Contour of wave $|u|$ obtained by the present method for Example 6 for particle distribution panel (f) of Fig. 1 with $\alpha = 0.7$ at $t = 0$ (a), 0.3 (b), 0.6 (c), and 1.0 (d).

Here, three different computing regions of panels (a), (d) and (f) of Fig. 1 in Example 6 are considered to further illustrating the flexibility of the proposed method for the 2D TF-GPE. The size of the computing region can be observed from Figs. 11–13. The comparisons of curves of wave $|u(0,y)|$ obtained by using different methods for Example 6 in a rectangular domain with $\alpha = 0.7$ are first demonstrated in Fig. 11 to show the reliability of the present method for the 2D TF-GPE. And then the proposed particle method is used to investigate the evolution of wave $|u|$ of Example 6 in irregular regions of panels (d) and (f) in Fig. 1 with $\alpha = 0.7$ as the time increases, which are illustrated in Figs. 12 and 13. From Figs. 11–13, it can be seen that i) the present results accord well with the FDM results in Fig. 11; ii) the peak values decreases with time in the case of the regular or irregular domain; iii) the proposed method can be flexibly extended to the 2D TF-NLSE/GPE in a complex irregular domain.

To sum up, it is reliable to predict the propagation of nonlinear waves by the present particle method for the 1D/2D TF-NLSE; the proposed method has more widely extended applications in the simulation of 2D problems in irregular computing regions than the grid-based method.

6. Remarks and conclusions

A flexible, effective, and accurate hybrid scheme (a local refinement corrected SPH method combined with FDM, which is called "LRCSPH-FDM") by combining a corrected SPH for spatial derivatives and the FDM scheme for the Caputo time fractional derivative is first proposed to solve the 2D time fractional nonlinear Schrödinger equation (TF-NLSE) in regular or complex irregularly shaped domains. Subsequently, the proposed purely meshless method is extended to predict the quantum mechanical character governed by the time fractional Gross–Pitaevskii equation (TF-GPE) in regular or complex irregular domains. Several examples are simulated by the present method and the results are compared with analytical solutions or FDM results. Meanwhile, the local refinement technique is adopted to reduce the numerical error, and nonregular particle distribution in rectangular or complex irregularly shaped domains is considered to demonstrate the flexible application ability and the merits of the purely meshless CSPH method for the TF-NLSE. Through the above numerical tests we can draw some conclusions below.

(I) The proposed method for the TF-NLSE has a second-order numerical accuracy, and it is reliable for simulating the TF-GPE without theoretical solutions.

(II) It is flexibly and easily implemented to simulate the TF-NLSE/GPE in non-uniform particle distributions or in complex irregularly shaped domains by the present method.

(III) The local refinement particle distribution can reduce errors and has a lower computational quantity than the global refinement approach.

(IV) The quantum mechanical property in the GPE can be effectively and accurately predicted by the proposed purely meshless method.

References

[1] Lavoie J L, Osler T J and Tremblay R 1976 *SIAM Rev.* **18** 240
[2] Podlubny I 1999 *Fractional Differential Equations* (New York: Academic Press)
[3] Mao Z P and Karniadakis G E 2018 *SIAM J. Numer. Anal.* **56** 24
[4] Hu J H, Wang J G and Nie Y F 2019 *Chin. Phys. B* **28** 100201
[5] Narahari Achar B N, Yale Bradley T and Hanneken John W 2013 *Adv. Math. Phys.* **2013** 290216
[6] Ray S S 2016 *Chin. Phys. B* **25** 040204
[7] Alzaidy J F 2013 *Amer. J. Math. Anal.* **1** 14
[8] Zhang J, Zhang X.D and Yang B H 2018 *Appl. Math. Comput.* **335** 305
[9] Deng W H 2009 *SIAM J. Numer. Anal.* **47** 204
[10] Wang H Q 2005 *Appl. Math. Comput.* **170** 17
[11] Bao W.Z, Jaksch D and Markowich P A 2003 *J. Comput. Phys.* **187** 318
[12] Bao W Z and Wang H Q 2005 *Commun. Math. Sci.* **3** 57
[13] Sulem C and Sulem P L 1990 *Appl. Math. Sci.* (New York: Spinger)
[14] Bao W Z and Wang H.Q 2006 *J. Comput. Phys.* **217** 612
[15] EI-Danaf T S, Ramadan M A and Abd Alaal F E I 2012 *Nonlinear Dyn.* **67** 619
[16] Wilson J P 2019 *Comput. Phys. Commun.* **235** 279
[17] Laskin N 2000 *Phys. Lett. A* **268** 298
[18] Laskin N 2002 *Phys. Rev. E* **66** 056108
[19] Naber M 2004 *J. Math. Phys.* **45** 3339
[20] Iomin A 2011 *Chaos, Solitons & Fractals* **44** 348
[21] Chen M, Guo Q, Lu D Q and Hu W 2019 *Commun. Nonlinear Sci. Numer. Simulat.* **71** 73
[22] Dong J P and Xu M Y 2008 *J. Math. Anal. Appl.* **344** 1005
[23] Li M Z, Ding X H and Xu Q 2018 *Adv. Differ. Equ.* **318** 1687
[24] Hicdurmaz B and Ashyralyey A 2016 *Comput. Math. Appl.* **72** 1703
[25] Chen X L, Di Y N, Duan J Q and Li D F 2018 *Appl. Math. Lett.* **84** 160
[26] Ozkan G 2015 *Chin. Phys. B* **24** 100201
[27] Edeki S O, Akinilabi G O and Adeosun S A 2016 *Commun. Math. Appl.* **7** 1
[28] Mohebbi A and Dehghan M 2009 *J. Comput. Appl. Math.* **225** 124
[29] Abdel-Salam E A B, Yousif E A and EI-Aasser M A 2016 *Rep. Math. Phys.* **77** 19
[30] Xu Y and Shu C W 2005 *J. Comput. Phys.* **205** 72
[31] Aboelenen T 2018 *Commun. Nonlinear Sci. Numer. Simulat.* **54** 428
[32] Shivanian E and Jafarabadi A 2017 *Numer. Methods Partial Differ. Equ.* **33** 1043
[33] Chen R Y, Nie L R and Chen C Y 2018 *Chaos* **28** 053115
[34] Azzouzi F, Triki H and Grelu P H 2015 *Appl. Math. Model.* **39** 1300
[35] Herzallah M A E and Gepreel K A 2012 *Appl. Math. Model.* **36** 5678
[36] Bhrawy A H and Abdelkawy M A 2015 *J. Comput. Phys.* **294** 462
[37] Zhang J W, Li D F and Antoine X 2019 *Commun. Comput. Phys.* **25** 218
[38] Khan N Alam, Jamil M and Ara Asmat 2012 *ISRN Math. Phys.* **2012** 197068
[39] Chen R Y, Tong L M and Nie L R 2017 *Physica A* **468** 532
[40] Lin Y M and Xu C J 2007 *J. Comput. Phys.* **225** 1533
[41] Gong Y Z, Wang Q, Wang Y S and Cai J X 2017 *J. Comput. Phys.* **328** 354
[42] Garrappa R, Moret I and Popolizio M 2015 *J. Comput. Phys.* **293** 115
[43] Zhuang P, Gu Y T, Liu F, Turner I and Yarlagadda P K D V 2011 *Int. J. Numer. Methods Eng.* **88** 1346
[44] Shivanian E 2015 *Int. J. Numer. Methods Eng.* **105** 83
[45] Basic J, Degiuli N and Ban D 2018 *J. Comput. Phys.* **354** 269
[46] Mohebbi A, Abbaszadeh M and Dehghan M 2013 *Eng. Anal. Bound. Elem.* **37** 475
[47] Liu G R and Liu M B 2003 *Smoothed Particle Hydrodynamics: A Meshfree Particle Method* (Singapore: World Scientific)
[48] Chen J K and Beraun J E 2000 *Comput. Methods Appl. Mech. Eng.* **190** 225

[49] Quinlan N J, Basa M and Lastiwka M 2016 *Int. J. Numer. Methods Eng.* **66** 2064
[50] Jiang T, Chen Z C, Lu W G, Yuan J Y and Wang D S 2018 *Comput. Phys. Commun.* **231** 19
[51] Jiang T, Huang J J, Lu L G and Ren J L 2019 *Acta Phys. Sin.* **68** 090203 (in Chinese)
[52] Li S F and Liu W K 2002 *Appl. Mech. Rev.* **55** 1
[53] Dehghan M, Abbaszadeh M and Mohebbi A 2014 *Cmes-Comp. Model. Eng.* **100** 399
[54] Tayebi A, Shekari Y and Heydari M H 2017 *J. Comput. Phys.* **340** 655
[55] Liu J M, Li X K and Hu X L 2019 *J. Comput. Phys.* **384** 222
[56] Liu M B and Liu G R 2010 *Arch. Comput. Methods Eng.* **17** 25
[57] Crespo A J C, Dominguez J M, Rogers B D and Gomez-Gesteira M 2015 *Comput. Phys. Commun.* **187** 204
[58] Sun P N, Colagrossi A, Marrone S and Zhang A M 2017 *Comput. Meth. Appl. Mech. Eng.* **315** 25
[59] Ren J L, Jiang T, Lu W G and Li G 2016 *Comput. Phys. Commun.* **205** 87
[60] Monaghan J J and Kocharyan A 1995 *Comput. Phys. Commun.* **87** 225
[61] Morris J P, Fox P J and Zhu Y 1997 *J. Comput. Phys.* **136** 214
[62] Jiang T, Lu L G and Lu W G 2014 *Comput. Mech.* **53** 977
[63] Yang X F, Peng S L and Liu M B 2014 *Appl. Math. Model.* **38** 3822
[64] Liu M B, Xie W P and Liu G R 2005 *Appl. Math. Model.* **29** 1252
[65] Zhang Z L and Liu M B 2018 *Appl. Math. Model.* **60** 606
[66] Gao G H, Sun Z Z and Zhang H W 2014 *J. Comput. Phys.* **259** 33
[67] Zhou X F, Wu C J and Guo G C 2018 *Phys. Rev. Lett.* **120** 130402
[68] Wang T C, Guo B L and Xu Q B 2013 *J. Comput. Phys.* **243** 382